Oxygen atoms and nitrogen molecules as spectroscopic probes for the temperature determination in non-equilibrium cryogenic helium plasma jets

R Boltnev, V Atrazhev, N Bonifaci, I Bykhalo, I Krushinskaya, V Khmelenko, D Lee, A Pelmenev, S Sheludiakov, N Sadeghi

Oxygen atom and nitrogen molecule as spectroscopic probes for the temperature determination of non-equilibrium cryogenic helium plasmas jet

R.E. Boltnev[1,2,3], V.M. Atrazhev[1], N. Bonifaci[4], I.B. Bykhalo[2], I.N. Krushinskaya[2], V.V. Khmelenko[5], D.M. Lee[5], A.A. Pelmenev[2], S. Sheludiakov[5], and N. Sadeghi[6]

[1] Joint Institute for High Temperatures, Russian Academy of Sciences, Izhorskaya str. 13/2, Moscow, 125412,

[2] Chernogolovka Branch of the N.N. Semenov Federal Research Center for Chemical Physics, Russian Academy of Sciences, Chernogolovka, 142432, Russia

[3] Moscow Institute of Physics and Technology, Dolgoprudnyi, Moscow region, 141701 Russia

[4] Laboratoire de Génie Electrique – G2Elab, Bât. GreEn-ER, 21 avenue des martyrs, CS 90624, 38031 Grenoble, France

[5] Institute for Quantum Science and Engineering, Department of Physics and Astronomy, Texas A&M University, College Station, Texas 77843, USA

[6] LIPhy (URA 5588) & LTM (URA 5129), Université Grenoble-Alpes & CNRS, Grenoble, 38402, France

Determination of the gas temperature in the afterglow plasma jet of pre-cooled helium propagating inside a dense helium vapor at 1.4 K is a difficult task. In this work we analyze the possibility of using the emission spectra from oxygen atoms and nitrogen molecules for deducing the local temperature of the gas. Oxygen is always present as a trace impurity (~ 1 ppm) in helium gas and strong emission of the atomic 777 nm triplet lines can be a good candidate because the energy gaps of 3.67cm^{-1} (T ~ 5.3 K) and 2.02 cm^{-1} (T ~ 2.9 K) between the sub-levels of its upper state O(^{5}P$_J$), with J = 1, 2 and 3, are comparable to the kinetic energy of atoms in a cryogenic environment. A detailed analysis of the kinetics of atoms in the O(^{5}P$_J$) state indicates that, due to the presence of small energy barriers in the He-O(^{5}P$_J$) transient molecule formed during the collision, population transfer between sub-levels is not efficient enough for the establishment of a Boltzmann equilibrium within the sublevels before the radiative decay of O(^{5}P$_J$) atoms. It was also shown that the temperature of a gas in non-equilibrium cryogenic helium plasmas containing at least 100 ppm of nitrogen can be determined from the rotational spectra of the 2-0 and 3-1 bands of the first positive system and the 8-3 band of the infrared afterglow system of molecular nitrogen. Application of PGopher software (1-T method) gives the rotational temperature of N_2 molecules averaged over the observation area and is optimal for the gas temperature determination in locally homogeneous plasmas or mapping the temperature in inhomogeneous plasmas with high spatial resolution. A home-made code to simulate rotational spectra with two temperatures (2-T method) allows determination of the temperature span within the observation area of an inhomogeneous plasma.

Keywords - cryogenic plasmas, atomic and molecular spectra, gas temperature determination

1. Introduction

The lack of information on the temperature of helium gas is a typical problem in experiments with non-equilibrium cryogenic helium plasmas, where the temperatures of heavy species (neutrals and ions) are less than 100 K, while the electron temperature is much higher, ~ 10000 K. In pure helium, the gas temperature determination by optical emission spectroscopy is not a simple task, despite the fact that many neutral and ionic states of He atoms and He_2^* molecules are involved in the energy circulation of cryogenic helium plasmas [1]. Population distributions in rotational levels of some excited states of molecular helium in cryogenic environments may show more than one peak and unacceptably high rotational temperature T_{rot}:

this was observed in the absorption spectra from the metastable $He_2(a^3\Sigma^+_u)$ state [2,3,4] and in the emission spectra of the $He_2(c^3\Sigma^+_g)$ state [5]. These facts reveal the presence of concurrent mechanisms for the population of the excited states and for the collisional transfers within rotational levels [6]. The observed high T_{rot} of the excited states probably results from the very short life times ~ 10 ns [7], reaching ~ 1 ns, for the high Rydberg states of He_2 [8]. It was shown that the rotational spectra of He_2^* molecules may be used for gas temperature measurements in the glow discharges at rather high pressure and current values [9,10] while a typical emission spectrum of the $d^3\Sigma^+_u$ - $b^3\Pi_g$ transition of He_2^* from a cryogenic helium plasma jet at T< 100 K is shown in Fig. 1. For quantum numbers $N' \geq 5$, the Boltzmann plot of the normalized rotational lines intensities, shown in the inset of Fig. 1, gives $T_{rot} \approx 760$ K which is much higher than the gas temperature. However, the much steeper decay of the intensities for lower N' values indicates a tendency for the collisional equilibrium between T_{rot} and the gas temperature for the low rotational levels of the $d^3\Sigma^+_u$ state. One exception only for cryogenic plasmas was reported in the literature for the He_2 excimer solvated in the liquid helium [11]: the lowest allowed rotational quantum state of the $d^3\Sigma_u^+$ state was exclusively populated.

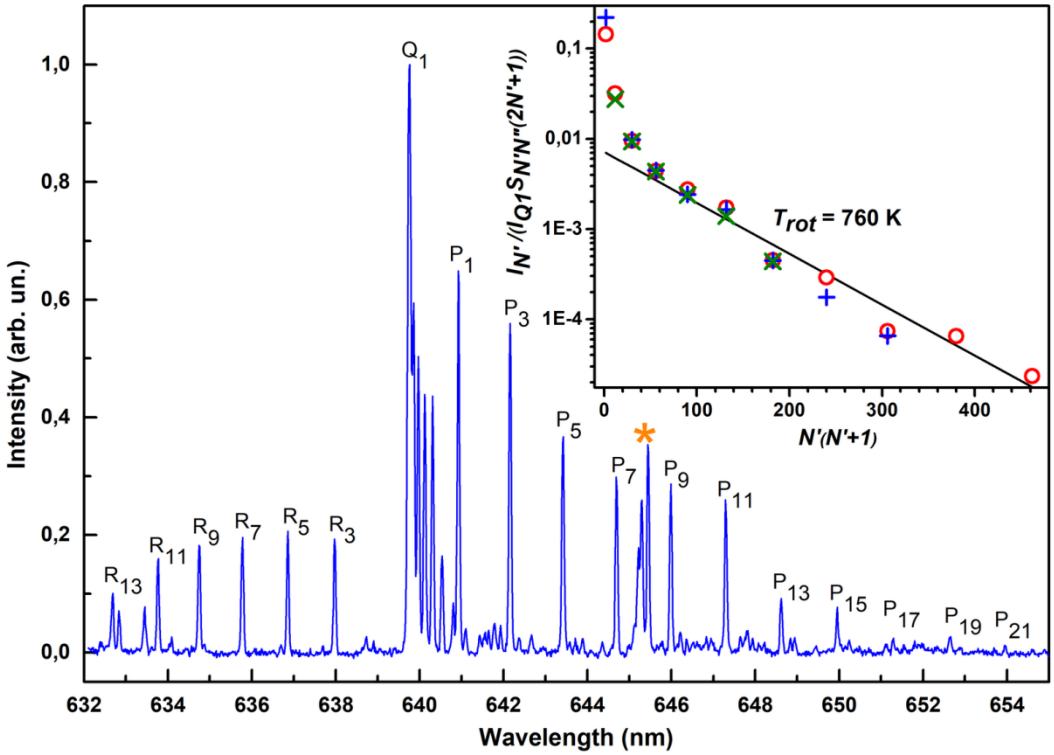

Fig. 1. Rotational structure of the emission spectrum of the $d^3\Sigma^+_u$– $b^3\Pi_g$ transition of He_2^* observed from the cold helium gas jet passed through an RF discharge region. The relative intensities (normalized by the Q1 branch intensity, the Honl-London and $(2N'+1)$ factors) of the P, Q, and R branches determined from the spectrum are shown by open red circles, blue and green crosses, respectively, in the inset. The black line represents a Boltzmann plot of the rotational level populations corresponding to $T_{rot} \approx 760$ K. An orange asterisk marks the oxygen atom triplet lines of the $3p^5P_{1,2,3}$– $5s^5S_2$ transitions at 645.6 nm in the main figure.

The presence of impurities in helium gas changes the emission spectra observed in different plasmas initiated by radiofrequency (RF), dielectric barrier discharge (DBD), corona, direct current (DC) discharges or by highly energetic particles [12,13,14,15,16,17,18,19,20]. Lowering the temperature of the helium gas usually causes decreasing of the impurity emission intensities accompanied by increasing of the emission intensity from the helium atoms and

molecules [14,15]. Nevertheless, fast cooling (for $\Delta T \approx 100$ K within time ~ 0.1 ms) of the helium plasma jet allows observation of intense emission from impurity species at temperatures ~ 10 K [12,16,18,21,22]. This peculiarity of non-equilibrium plasmas may be used for the estimation of the cryogenic jet temperature from the optical spectra of the impurity particles. For instance, the ratio of the emission intensities of the NO molecule doublet, corresponding to the transitions $B^2\Pi_{1/2} - X^2\Pi_{1/2}$ and $B^2\Pi_{3/2} - X^2\Pi_{3/2}$, has allowed Popov *et al* to estimate a temperature of about 20 K in the cryogenic plasma jet [22]. Moreover, the rotational temperature ≈ 5 K of NH_3 molecules, very close to the cell temperature of 3.8 K, was measured [17] in so-called a cryo-microplasma, a specific type of plasma in cryogenic conditions within a very geometrically restricted discharge volume (< 1 mm^3) [23,24].

In this work we compare two methods, based on the optical emission spectroscopy, intended for the temperature determination in the cryogenic non-equilibrium plasmas. Both of them use the natural impurities always present in helium gas, namely oxygen and nitrogen molecules. The former uses the relative intensities of the oxygen atom triplet at 777 nm, corresponding to the $3s^5S_2$ - $3p^5P_{1,2,3}$ transitions. The latter uses the rotational structure of the first positive (1^+) system of the molecular nitrogen, corresponding to the $B^3\Pi_g - A^3\Sigma_u^+$ transition [25,26]. We will present the spectra recorded at different locations of the cryogenic helium plasma jet and the temperatures deduced from their comparison with synthetic spectra. Then the reliability of these probes for the determination of the kinetic temperature in cryogenic (T < 100 K) non-equilibrium plasmas will be discussed.

2. Experimental setup

An experimental approach using injection of the gaseous helium jet containing a small admixture ~ 1 % of impurities into superfluid helium (He II) was developed in the early 1970s [27]. The experimental setup was described in detail elsewhere [28]. The gas mixture passed through a quartz capillary of about 3 mm inner diameter and was pre-cooled by liquid nitrogen (see Fig. 2). Electrodes were located around the quartz capillary and powered with an RF generator (53 MHz, 60-90 W) providing a discharge, which ionized the gas, produced metastable helium atoms, and dissociated impurity molecules. Under a small pressure gradient ($\Delta P \approx 260$ Pa) across the capillary, a well-formed jet is created after the passage of the gas mixture through a small orifice (0.75 mm diameter) at the end of the capillary. The typical velocity of the jet at the exit of the orifice, whose temperature is 100 K, is about 200 m/s at a flow rate of $5 \cdot 10^{19}$ atoms/s. As the already pre-cooled jet expands into the helium cryostat, the whole gas (helium + impurities) in the jet is cooled efficiently by the dense helium vapor and the temperature of atoms and molecules in the jet drops from about of 100 K near the orifice down to 1.45 K at the surface of the superfluid He II in the collection beaker. Similarly, as the helium vapor becomes denser with the decreasing temperature, the jet velocity should decrease with increasing of the distance from the orifice. The beaker was placed 25 mm below the capillary orifice and a constant liquid helium level in the beaker was provided by a fountain pump located at the bottom of the helium dewar [28].

In the experiment, we used research grade “pure” helium from Linde Electronics & Specialty Gases with 99.9999% purity. The oxygen content of the helium cylinder is ~ 1 ppm. Even such a small admixture of oxygen is easily observable in the “pure” helium plasma jet [18], as seen in Fig. 1a. In some experiments, the gas is a premixed He with up to 0.5% volume of N_2. The flux of the gas entering the cryostat is preset by a Brooks Instrument 5850E flow controller. The typical flux of $5 \cdot 10^{19}$ atoms/s creates a crater in the HeII surface easily observable due to the strong green

emission (Fig. 2a), while at a lower flux of $1 \cdot 10^{19}$ atoms/s, we can see of a bright radial plasma layer spreading along the cold liquid surface (Fig. 2b).

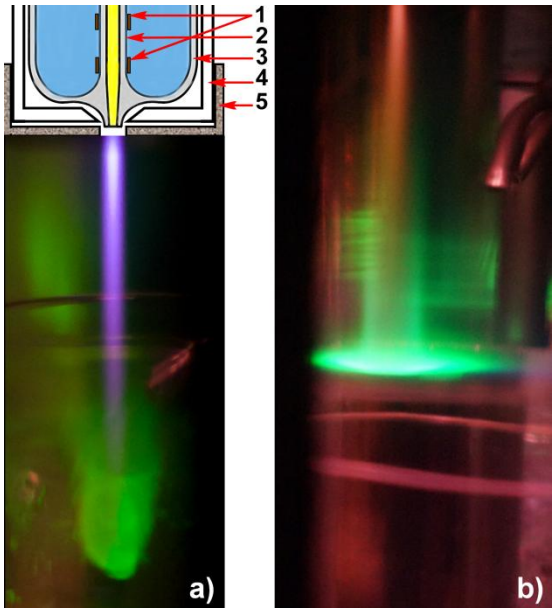

Fig. 2.Experimental set-up: a) green emission of oxygen atoms from a crater on the HeII surface formed by a "pure" helium jet passed through the RF discharge; a scheme of the discharge zone is shown at the top: 1 –electrodes, 2 – quartz capillary, 3 – quartz tube, 4 – vacuum jacket of the source, 5 – thermal shield; b) helium-nitrogen plasma jet scattered on the HeII surface (gas mixture $[N_2]/[He]=1/100$).

The temperature of liquid helium in the cryostat approximately 1.45 K corresponding to its saturated vapor pressure ≈ 400 Pa was maintained by adjusting the pumping speed of helium vapor from the cryostat. This temperature was measured by a Lake Shore germanium thermometer. The optical emission from different parts of the plasma jet could be collected by a lens which forms the image of the jet onto the entrance face of an optical fiber bundle. In this way the emission was collected from areas with different temperatures along the jet length and diameter. The fiber location (height) was determined by its position above the HeII level in the beaker. The fiber is split into two separate channels, one of which was attached to an Ocean Optics spectrometer and the other to an Andor Shamrock SR500 spectrograph. The Ocean Optics spectrometer HR2000+ was used for recording the spectra over a broad wavelength range (200–1100 nm) with a spectral resolution of 1.3 nm, whereas the Andor spectrograph, backed with a Newton EMCCD camera, was used to obtain high resolution spectra, with a spectral resolution of 0.05 nm.

3. Temperature probes for cryogenic helium plasma jets

We have chosen two different species, present as natural contaminants in helium gas, as temperature probes in the cryogenic helium plasmas. The first one is an oxygen atom, whose emission is greatly enhanced at cryogenic temperatures [18,29], and the second one is a nitrogen molecule, for which the rotational structure of the bands of the 1^+ system can be an indication of the gas temperature [25,26]. However, to understand the variation along the plasma jet of the relative intensity changes of the different components of oxygen 777 nm line and of the distribution in rotational lines of the $N_2(1^+, 2\text{-}0)$ band, it is also necessary to analyze mechanisms responsible for the production of O atoms and N_2 molecules in the excited states of these

transitions, and the effective lifetimes of these states, as well as the mechanisms of collisional transfers between the neighboring fine-structure or rotational levels. In the following, we will successively discuss advantages associated with each of these probes by analyzing the origin of O 777 nm lines and $N_2(1^+, 2\text{-}0)$ band emissions, and will show examples of observed spectra and finally will discuss the kinetics of $O(^5P_J)$ atoms and $N_2(B^3\Pi_g)$ molecules.

3.1 $O(^5P_J)$ atoms as temperature probes

The emission intensity of atomic oxygen lines is strongly enhanced in cryogenic environments at $T \sim 10$ K. When O_2 concentration in the helium carrier gas is lower than 0.1 % (1000 ppm), molecular oxygen is completely dissociated by the discharge. As shown in Figs. 1 and 2a, the oxygen content of about 1 ppm in a helium jet is enough to produce the emission of the oxygen lines. The recorded emission spectra contains many spectral lines of atomic oxygen, including the $3s^5S_2 – 3p^5P_{1,2,3}$ transitions at 777 nm [18]. The oxygen triplet lines at 777.19, 777.42 and 777.54 nm are good candidates for the temperature determination because the energy gaps between the fine-structure levels of their upper states $3p^5P_{3,2,1}$ equal to 3.67cm^{-1} ($T \sim 5.3$ K) between J=3 and J=2, and 2.02 cm^{-1} ($T \sim 2.9$ K) between J=2 and J=1, respectively, are comparable to the kinetic energy of particles in cryogenic medium (see the state diagram in Fig. 3). Such a level configuration makes the system particularly sensitive to the temperature changes below 30 K.

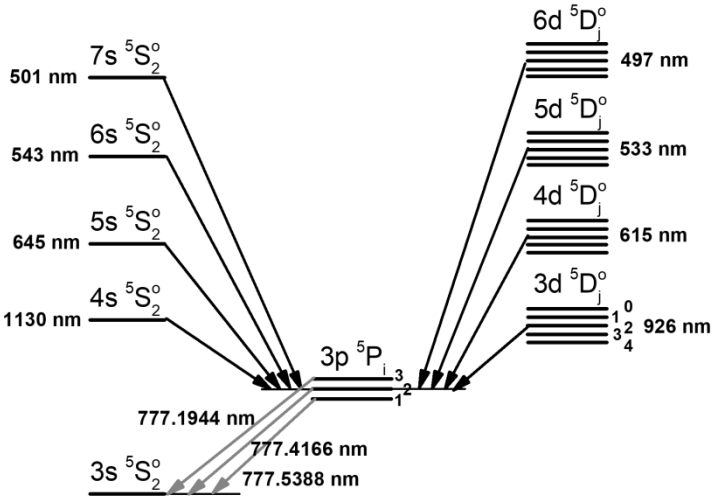

Fig. 3. Scheme of the oxygen atom energy states populating the $3p^5P_{1,2,3}$ levels emitting to the $3s^5S_2$ state, and the transition wavelengths.

The spectra of the triplet lines, simulated under the assumption of Boltzmann equilibrium between fine-structure levels, are shown in Fig. 4a for temperatures 20, 15, 10, and 5 K. For instance, the experimental spectrum detected from the bottom part of the plasma jet formed by "pure" helium gas, with no nitrogen admixture, passed through a RF discharge area is shown in Fig. 4b (green line) along with its best fit, corresponding to 12.5 K (black dotted line).The triplet lines are well resolved at the spectral resolution of a spectrometer better than 0.1 nm (see Fig. 4b). Usually we were not able to observe the 777 nm emission in the spectra of helium plasma jets containing more than 0.1 % molecular nitrogen.

To simulate the intensities of the triplet lines at different temperatures, we used the level energies 86631.45, 86627.78, 86625.76, and 73768.2 cm^{-1}, respectively, for the $^5P_3$, $^5P_2$, $^5P_1$, and

$3s^5S_2$ states, the transition probabilities $3.325 \cdot 10^7$, $3.293 \cdot 10^7$,and $3.306 \cdot 10^7$ s^{-1}, and the wavelengths 777.1944, 777.4166, and 777.5388 nm, correspondingly [30].

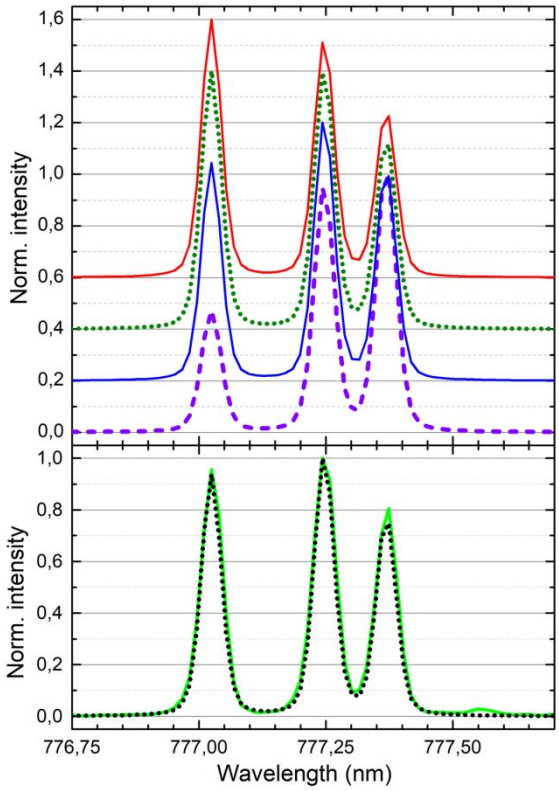

Fig. 4. Dependence the relative intensities of the oxygen fine-structure triplet lines at 777 nm on the gas temperature: a) synthetic spectra for temperatures 20, 15, 10, and 5 K, red, dotted green, blue, and dashed violet lines, respectively, calculated assuming full Boltzmann equilibrium of the sub-levels; b) experimental spectrum (green line) recorded from the bottom of the plasma jet, near the HeII surface, together with the simulated one for T = 12.5 K (dotted black line).

3.2 Kinetics of $O(^5P_J)$ atoms

The oxygen lines at 777 nm are always present in the emission spectra of atmospheric pressure (AP) room temperature helium plasmas, even when using "pure" helium gas with less than a few ppm impurity [31,32,33,34]. In these plasmas, the commonly proposed mechanisms for the production of $O(^5P_J)$ atoms are electron impact excitation of the ground state O atoms and the dissociative excitation of the ground state O_2 molecules by $He(^3S_1)$ and/or $He_2(a^3\Sigma^+_u)$ metastable species [34,35,36]. Nayak *et al* have recently measured lifetimes of 4 and 9 μs for $He(^3S_1)$ and $He_2(a^3\Sigma^+_u)$ metastable species, respectively, in an AP helium RF plasma in which the amount of the total impurities (O_2, N_2 and H_2O) was lower than 10 ppm [37]. Considering the rate coefficients for the quenching of these metastable species by nitrogen and oxygen, which are in the range of $1 \cdot 10^{-16}$ m^3/s [38], with 200 ppm impurity in the helium gas jet, these metastable species should survive for about 10 mm inside the cryostat and partly reach the He II surface. However, besides contribution from $He(^3S_1)$ and $He_2(a^3\Sigma^+_u)$, one can also imagine other production mechanisms of $O(^5P_J)$ atoms in the afterglow. One of them could be the VUV photo-excitation of O_2 by the Hopfield continuum of helium, which extends from 60 to 110 nm [39]. This continuum emission $He_2(A^1\Sigma^+_u - X^1\Sigma^+_g)$ from the RF discharge inside the quartz tube exits from the small orifice in its bottom and propagates all along the gas jet flow in the cryostat. The helium medium is fully transparent to this emission because the lower state of the transition,

$X^1\Sigma^+_g$, is dissociative, while photons with $\lambda < 78$ nm have enough energy to induce the photo-dissociation of O_2 into the $O(^5P_J)$ state. As was observed by Reuter *et al*, VUV photons belonging to the O and O_2 transitions are also emitted from the oxygen impurity present in He discharge [40]. These photons can also be absorbed by O and O_2 of the helium jet, producing $O(^5P_J)$ atoms. The other possibility for producing excited O atoms could be electron-ion and/or ion-ion recombination within the gas jet. It is well known that different types of positive and negative oxygen ions are produced in helium discharges containing an O_2 impurity [41,42,43]. These charged particles are transported with the gas flow into the cryostat, where the dissociative electron-ion recombination of metastable ions $O_2^+(a^4\Pi_u)$ and/or ion-ion recombination O_x^+-O_y^-, with x=1-2 and y=1-3, can also produce $O(^5P_J)$ atoms. Nevertheless, whatever the production mechanism, considering the large number of pathways there should be a high tendency for the fine-structure sub-levels of the $O(^5P_J)$ state to be populated with relative probabilities close to their statistical weights: $2J+1$.

Considering almost identical transition probabilities for the all 3 components of the 777 nm triplet [30], their relative intensities are proportional to the population density of sub-levels, N_J. In the steady-state, the rate equations which describe the populations N_J can be written:

$$\frac{\partial N_J}{\partial t} = S_J - \left(A_J + k_{He}\cdot[He] + \sum_n k_{q,n}\cdot[Q]\right)\cdot N_J + \sum_{J'}\left(k_{J',J}\cdot N_{J'} - k_{J,J'}\cdot N_J\right)\cdot[He] = 0 \qquad (1)$$

where J and J' (=1, 2 or 3) refer to the three sublevels, S_J is the population rate of the sublevel J; the second term represents the depletion of the sublevel J by radiative decay and quenching by helium atoms of density [He] (transfers out of the 3 sublevels) and by species "q" (N_2 and O_2) of density [Q]; and the 3rd term corresponds to collisional transfers, with rate coefficients $k_{J',J}$, between sublevels, induced by helium atoms. It is obvious that the $k_{J,J'}$ coefficients are related to each other by the principle of detailed balancing:

$$k_{J',J} = k_{J,J'}\frac{2J+1}{2J'+1}exp\left(-\frac{E_J - E_{J'}}{kT_g}\right) \qquad (2)$$

where E_J is the J levels' energy and T_g is the gas temperature. Solving together the 3 rate equations of the sublevels for deducing the relative densities N_J is beyond the scope of this paper because many of the rate coefficients are not known. However, the analysis of the 2nd term of Eq. (1), which is the decay frequency of N_J, and its 3rd term, the populations mixing frequency of the sublevels, can provide some insight relative to the evolution of the density ratios with the gas temperature; this latter being continuously decreasing from the exit of the discharge tube until the surface of He II.

We know of one experiment in which cross-sections $\sigma_{J,J'}$ of $2.5\cdot10^{-19}$, $4.4\cdot10^{-19}$, and $6\cdot10^{-19}$ m^{-2} have been measured at 300 K for the exoenergetic transfers $k_{3,2}$, $k_{2,1}$ and $k_{3,1}$, respectively [44]. With 400 Pa He pressure in the cryostat, if no T_g dependence of cross section is assumed, the value $\sigma_{J,J'}=5\cdot10^{-19}$ m^{-2} will lead to transfer frequencies of $7\cdot10^7$, $1.4\cdot10^8$, $2.4\cdot10^8$, and $4\cdot10^8$ s^{-1} at temperatures of 300, 77, 25, and 10 K, respectively. Consequently, if the 29 ns radiative life time [45] of $O(^5P_J)$ was not shortened by its collisional quenching, $O(^5P_J)$ atoms of the cold-jet would suffer several collisions during their lifetime, inducing transfers between the sub-levels and leading to the equilibrium of their populations with T_g.

Belikov *et al* have measured the quenching coefficient $k_q(O_2)$ of $O(^5P_J)$ by O_2 and predicted its $1/T^{0.8}$ variation with the temperature [46]. Also, Dagdigian *et al* have reported on comparable rate coefficients for the quenching of $O(^3P_J)$ by N_2 and O_2 molecules and of $O(^5P_J)$ by O_2 [47]. Without any other information in hand, we consider a rate coefficient for the quenching of $O(^5P_J)$ by N_2 similar to the value reported in [46] for its quenching by O_2. For the numerical estimates, we will take the conservative value $k_q=1\cdot10^{-15}$ m^3s^{-1}, measured in [46] at T = 77 K and will

consider 100 ppm of N_2 in He (value used in the present work when recording together both oxygen and nitrogen spectra). At the exit of the discharge tube, with $T \approx 100$ K we deduce a quenching frequency of about $4 \cdot 10^4$ s^{-1} and considering the $T^{-0.8}$ dependence of the rate coefficient, we obtain $3 \cdot 10^5$ s^{-1} and $1.5 \cdot 10^6$ s^{-1} at T = 25 and 10 K, respectively. These quenching rates are more than an order of magnitude smaller than the radiative decay frequency of the $O(^5P_J)$ state and thus, the quenching by N_2 and O_2, whose content under the conditions of Fig. 4 was 1 ppm, can be neglected in Eq. (1).

We also couldn't find any publication on quenching of the $O(^5P_J)$ state by He atoms. As a general rule, the rate coefficients for the quenching of electronically excited atoms by He and Ne are much smaller than for the heavier rare-gases, Ar, Kr, and Xe [48]. This probably results from smaller polarizability of the former and the less attractive nature of $O(^5P_J)$-He potential curves. We should emphasize that, due to the zero spin momentum of He and the total spin conservation rule during a collision, only transfers to the other quintet, $3s^5S_2$ state have a non negligible probability. But with 1.84 eV energy gap between states, the curve crossing between He-O potentials originated from $3s^5S_2$ and $3p^5P_J$ states, required for the population transfer, is hardly acceptable. Taking a conservatively large value of $k_{He} = 1 \cdot 10^{-17}$ m^{-3}, we deduce quenching frequencies of $4 \cdot 10^6$, $1.2 \cdot 10^7$, and $3 \cdot 10^7$ s^{-1} at 77, 25 and 10 K, respectively, which are at most comparable to the radiative decay frequency of the $O(^5P_J)$ state.

Thus, under the assumption of the independence of $\sigma_{J,J'}$ cross-sections on T_g, the population mixing times by He of the sub-levels will be much shorter than the lifetime of the $O(^5P_J)$ state and the Boltzmann equilibrium assumption will be a good approximation in helium plasma jets with N_2 content less than 1000 ppm. The simulated profiles of Fig. 4 have been obtained under this assumption, with almost infinite lifetime of $O(^5P_J)$ state. In section 4 "Discussion" of the paper, however we will see that the constant $\sigma_{J,J'}$ hypothesis is highly questionable.

3.3 $N_2(B^3\Pi_g)$ molecules as temperature probes

The emission spectra from excited states of N_2 molecule, especially the first positive (1^+) and the second positive (2^+) systems, are very popular for the gas temperature determination in plasmas [49,50,51,52]. In AP room temperature helium plasmas, the emission intensity of the 1^+ is often very weak and the 2^+ systems is commonly used for the determination of T_{rot} [53,54,55]. However, approximate 10 μs radiative life time of the upper state of the 1^+system, $B^3\Pi_g$ [56,57], should be much more favorable for reaching the translation-rotation equilibrium than in the $C^3\Pi_u$, the upper state of the 2^+ transition, whose radiative life time is only ≈ 40 ns [57]. The longer life time of the $B^3\Pi_g$ state can be an advantage for the establishment of a rotation-translation equilibrium, induced by collisions with the helium bath gas even at pressures as low as a few tens of mTorr [58].

Another advantage of the 1^+ system of molecular nitrogen is its high emission intensity in cryogenic plasmas, even in the afterglow [19,59]. Even at the nitrogen content less than 1000 ppm we were able to see spectra of both atomic oxygen and molecular nitrogen. It is worth noting that cooling down the plasma jet enhances the emission intensity of molecular nitrogen: up to seven spectroscopic systems of N_2 and N_2^+ have been observed from the bottom, coldest part of the plasma jet [19]. The accumulation of molecules in the lowest rotational levels, resulting from collisional transfers by cold atoms of the cryogenic helium, simplifies the rotational structure of the bands and allows one better distinguishing spectra corresponding to different systems, even if they are within a few nm of each another.

The rotational structures of molecular nitrogen spectra were synthesized by two means: the PGOPHER program for simulating and fitting rotational, vibrational, and electronic spectra of molecules [60,61] in which full Boltzmann equilibrium at one rotational temperature is assumed, and a home-made code to simulate rotational spectra with two temperatures. The latter allows us to make an estimation of the temperature span between the outer (cold) part of a plasma jet and its hot core.

The experimental spectra detected from the top, middle, and bottom parts of the plasma jet formed by the gas mixture $[N_2]/[He] = 1/200$ passed through the RF discharge area are shown in Fig. 5 along with their best simulations. The 2-0 band of the 1^+ system is the main spectral feature and its intensity increases upon lowering the jet temperature [19]. The 8-3 band of the infrared afterglow (IRA) system, corresponding to the $B'^3\Sigma_u$- $B^3\Pi_g$ transition of molecular nitrogen becomes observable at the plasma jet temperature below 50 K within the spectral range between 778 and 780.5 nm (in the right side of the vertical dashed line). The intensity scale was diminished within this range by 15 fold in Fig. 5.

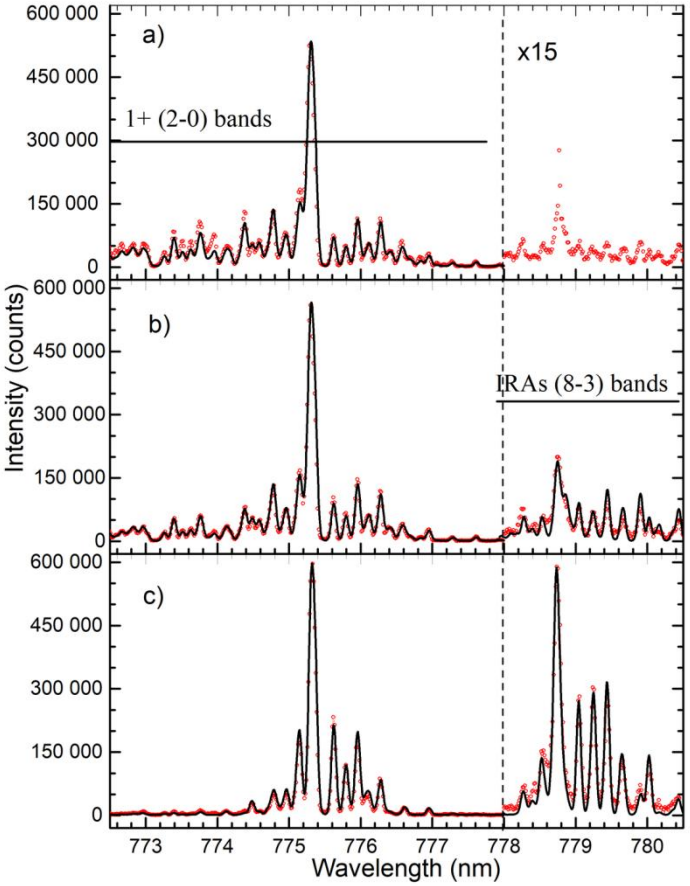

Fig. 5. The best simulations (black lines) of experimental spectra (shown by red circles) of N_2 molecules detected from the top, middle, and bottom parts (a, b, and c figures, correspondingly) of the plasma jet formed by the gas mixture $[N_2]/[He] = 1/200$ passed through RF discharge area.

The temperatures evaluated from the rotational structures of the 2-0 band of the 1^+ system detected from the top, middle, and bottom parts of the jet are 50 K, 38 K, and 14.5 K, respectively, in Figures 5a, 5b, and 5c. The temperatures evaluated from the rotational structures of the 8-3 band of the infrared afterglow system are 35 K and 11 K for the middle and bottom parts of the jet. The spectrum the 8-3 band detected from the top part is very weak for temperature determination. One can see no overlapping of the bands due to the depletion of their rotational

temperatures at these temperatures. Estimated uncertainties associated with temperatures deduced from the band 2-0 of the 1+ system and the band 8-3 of IRA system are 10 % and 20 %, correspondingly.

Usually we were not able to observe the oxygen atom triplet in the spectra of helium plasma jets containing more than 0.1% molecular nitrogen. Molecular nitrogen spectra were still observable from plasma jets at nitrogen content as low as 50-100 ppm in the helium gas. At nitrogen contents less than 1000 ppm we were able to see spectra of both atomic oxygen and molecular nitrogen. A strong depletion of the rotational structure in the spectrum of molecular nitrogen allows us to easily distinguish it from the triplet lines of atomic oxygen. Examples of such spectra along with their interpretations are shown in Fig. 6. The rotational spectrum of the 2-0 band of the 1^+ system of molecular nitrogen consists mainly of the branches Q_{11}, Q_{12}, Q_{13}, P_{11}, P_{12}, P_{13}, R_{11}, and R_{12}. The positions of these sequences' lines corresponding to the transitions from the different *J*" levels are shown with blue triangles down, magenta diamonds, violet triangles left, black squares, red circles, green triangles up, orange triangles right, and olive circles, respectively. The branch R_{13} is not shown in Fig. 6 because the exclusively small values of the Honl-London factors for this branch [26,62,63]. One can see that the transitions mainly from the sublevel $B^3\Pi_{0g}$ were observed from the middle part of the plasma jet. The rotational temperature of 30 K was estimated from this spectrum.

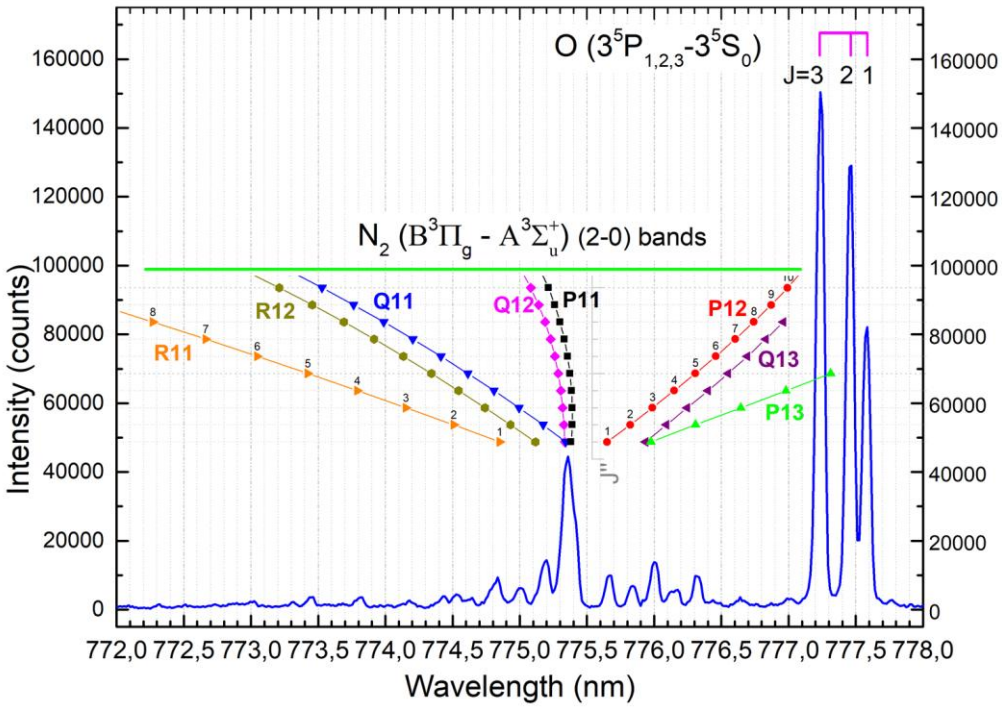

Fig. 6. Experimental spectra of the oxygen atom triplet and the rotational bands of the $B^3\Pi_g$,v=2 – $A^3\Sigma_u^+$,v=0 transition of N_2 molecule detected from the middle part of a plasma jet (gas mixture $[N_2]/[He]=1/10000$).

Comparing spectra shown in Figures 5 and 6, we point out the absence of oxygen 777 nm lines in the former ones. Due to the presence of large amount of nitrogen (0.5%) in helium gas, all He^+ and He_2^+ ions, as well as $He(^3S_1)$ and $He_2(a^3\Sigma^+_u)$ metastable species, generated in the discharge are immediately converted to N_2^+ ions by charge transfer and Penning ionization reactions [32]. Thus the primary channels for the production of electronically excited O atomsby helium metastable species, like dissociative excitation of O_2 or electron-O_2^+ dissociative

recombination, occurring at low N_2 content (and high helium ions and metastables densities) will be blocked. Observation of the spectra of the oxygen atom triplet at 777 nm simultaneously with the 2-0 band of the 1^+ system of molecular system allows us to compare directly the temperatures estimated from the spectra detected from the emission along the jet.

3.4 Kinetics of N_2 ($B^3\Pi_g$) molecules

In the same way as for O(^{5}P) atoms, $N_2(B^3\Pi_g)$ molecules of the cryogenic helium jet are produced from the long-lived species present in the afterglow. However, the reaction of atomic and molecular helium metastables with N_2 is known to result in Penning ionization and formation of $N_2^+(B^2\Sigma)$ ions [64,65] and thus, it cannot be the direct channel for the formation of $N_2(B^3\Pi_g)$ molecules. But, besides the photo-excitation from $N_2(X)$, electronically excited N_2 molecules can also be produced by electron-ion dissociative recombination of N_3^+ and N_4^+ ions generated by the 3-body reaction of N^+ and N_2^+ ions with N_2 and He [32,66]. However, the most expected reaction for the formation of $N_2(B^3\Pi_g)$ molecules is the 3-body recombination of two N(^{4}S) atoms [67,68], resulting from the dissociation of N_2 in the RF discharge and transported by the gas flow jet. Theoretical estimations predicted that the $A'^5\Sigma_g^+$ state of N_2 molecules is populated more efficiently due to recombination of nitrogen atoms in the ground state N(^{4}S) at lower temperatures: the rate constant for the formation the $A'^5\Sigma_g^+$ state at T = 4 K is about one order of magnitude larger than that at 300 K [69]. It is well established that, $N_2(A'^5\Sigma_g^+)$ molecules, the primary product of the recombination reaction N(^{4}S) + N(^{4}S) [69,70], are then transferred to the coupled group of triplet states: $G^3\Delta_g$, $B^3\Pi_g$, $W^3\Delta_u$, $B'^3\Sigma_u$, and $A^3\Sigma_u^+$ [71,72,73,74]. Populations of these 5 states being strongly coupled by collisional-radiative processes and due to the largest transition probability of the 1^+ emission from the $B^3\Pi_g$ state [57], a significant part of the molecules formed by N-N recombination will show-up in the emission intensity of the 1^+system. Formation of $N_2(B\,^3\Pi_g)$ can also occur through the interaction between $N_2(A\,^3\Sigma^+_u)$ and $N_2(X\,^1\Sigma^+_g, v\geq 5)$ molecules [75], and in energy pooling reactions between $N_2(A\,^3\Sigma^+_u, v=0,1)$ molecules [76]. This is also true after production of N_2 molecule in any of the above cited triplet states by other excitation mechanisms, such as VUV photoexcitation or electron-ion recombination. Considering the complex formation mechanisms of $N_2(B^3\Pi_g;v=2)$ molecules, it is hard to imagine a rotation level selectivity in its nascent population.

To analyze the kinetics of N_2(B;2) molecules within the rotational levels, one can write equations similar to Eq. (1), in which $N_{\Omega,J}$ will refer to the population of rotational level J of the spin coupling Ω sub-levels. In the steady-state, the rate equations describing the populations of rotational levels, $N_{\Omega,J}$ can be written as:

$$\frac{\partial N_{\Omega,J}}{\partial t} = S_{\Omega,J} - \left(A_{\Omega,J} + k_{He}\cdot[He] + \sum_n k_{q,n}\cdot[Q]\right)\cdot N_{\Omega,J} + \sum_{J'}\left(k_{\Omega,J',\Omega,J}\cdot N_{\Omega,J'} - k_{\Omega,J,\Omega,J'}\cdot N_{\Omega,J}\right)\cdot [He] = 0 \quad (3)$$

where Ω (=0, 1 and 2) refers to the total angular momentum of electrons of the three sublevels [77], $S_{\Omega,J}$ is the population rate of the sublevel J, and $A_{\Omega,J}$ is the Einstein coefficient of the N_2(B;2-A;0) transition, which is identical for all Ω and J values. The second term represents the depletion of the rotational level J by radiative decay and quenching by helium (transfers out of the spin sublevel Ω) and by species "q" (N_2 and O_2) of density [Q]; and the 3rd term corresponds to collisional transfers induced by He atoms, whose density is [He], between J and J' rotational levels, with rate coefficients $k_{\Omega,J',\Omega,J}$. We have considered that collisional transfers between Ω sublevels are negligible, similar to what was observed in the $N_2(C^3\Pi_u)$ state by argon [78].

Hereafter, we assume the $k_{\Omega,J',\Omega,J}$ as identical for all three Ω spin sublevels and hence the subscript Ω will be omitted. A quenching rate coefficient for N_2(B) by helium k_{He} ~10^{-18} m^3s^{-1} at room temperature has been reported by Piper [79], who also indicated a rate coefficient of k_{N2}=3.10^{-17} m^3s^{-1} for its quenching by N_2 molecules. Also, rate coefficients in the range of 10^{-17} m^3s^{-1} have been measured for the transfer to the N_2(W) state, induced by N_2, argon or neon [73,80]. Neglecting the contribution from N_2, and assuming the non T_g dependence of the cross section, which thus involves a k_{He} ~$(T_g/300)^{0.5}\cdot10^{-18}$ m^3s^{-1} variation of the k_{He} with the gas temperature, the estimated helium collision induced lifetime of N_2(B;2) inside the cryogenic helium jet will be about 5, 3, and 2 μs at 77, 25 and 10 K, respectively. These lifetimes are comparable to the few μs radiative life time of the N_2(B) state [57]. Concerning population transfers between rotational levels, we couldn't find any publication reporting on $k_{J,J'}$ coefficients in the N_2(B) state induced by He. Setser *et al* have found a transfer rate coefficient of about 10^{-16} m^3s^{-1} between rotational levels of the $N_2(C^3\Pi_u)$ state by argon [78]. Also, comparable $k_{J,J'}$ coefficients have been reported for the excited states of several diatomic molecules in collision with rare gas atoms, but also N_2 and H_2 [81,82,83,84 and references therein]. With $k_{J,J'}$ about 100 times larger than k_q, one can expect about hundred *J*-transferring collisions during the lifetime of N_2(B) molecule and thus a complete Boltzmann equilibrium between its rotational levels. However, according to the above cited works, the state-to-state rotational transfer rate coefficients, $k_{J,J'}$, decrease with increasing energy gap between initial and final rotational levels, $\Delta E_{J,J'} = |E_J - E_{J'}|$. Several scaling laws have been proposed [81,82,83,85,86], including the power decay law:

$$k_{J,J'} \propto \Delta E_{J,J'}^{-\beta} \quad (4)$$

where β is a positive constant, very close to 1 [82,83]. With E_J=$BJ(J+1)$, where B = 1.592 cm^{-1} is the rotational constant of N_2(B;2) [57], the energy gap between successive rotational levels is $|\Delta E_{J,J+1}| = 2B(J+1)$ and thus, the state-to-state transfer rate coefficient becomes smaller with increasing *J*. In addition, the sum $\sum_{J'} k_{J,J'}$ of all coefficients out of the *J* level is larger for smaller rotational numbers [82,87], since there is a wider availability of *J'* levels because of the smaller energy gaps.

In conclusion, under our experimental conditions of the cryogenic helium jet, the populations of low *J* levels of the N_2(B;2) state can reach the Maxwell–Boltzmann distribution represented by a rotational temperature $T_r = T_g$, while the populations of high *J* levels may give $T_r \geq T_g$. This fact can be observed in the $N_2(1^+,2\text{-}0)$ band by a close observation of its low wavelength region, where rotational lines originated from high rotational levels are present. Figure 7 duplicates Fig. 5a, but with the wavelength scale starting from 770 nm, instead of 772.5 nm. There our experimental data (shown by black circles) are presented in Fig. 7 along with spectrum simulated with two different rotational distributions (red line) and the spectrum simulated for full Boltzmann equilibrium at T_r = 50 K (blue line), as in Fig. 5a. The former considers 2 rotational temperature distributions, with density N_J of the levels given by:

$$[N_J] \propto (2J+1)\left[\exp\left(-\frac{E_J}{kT_r^L}\right) + R\left(\frac{T_r^L}{T_r^H}\right)\exp\left(-\frac{E_J}{kT_r^H}\right)\right] \quad (5)$$

where *R* is a coefficient which indicates the relative contributions of the two terms of (5) and T_r^L=30 K and T_r^H=120 K, which in the case presented in Fig.7, are representative of the density distribution in the low and high rotational levels, respectively. It is clearly evidenced that the 2-T simulation reproduces much better the recorded intensities of the lines originating from high rotational levels, lines which are present in the short wavelength side of the spectra.

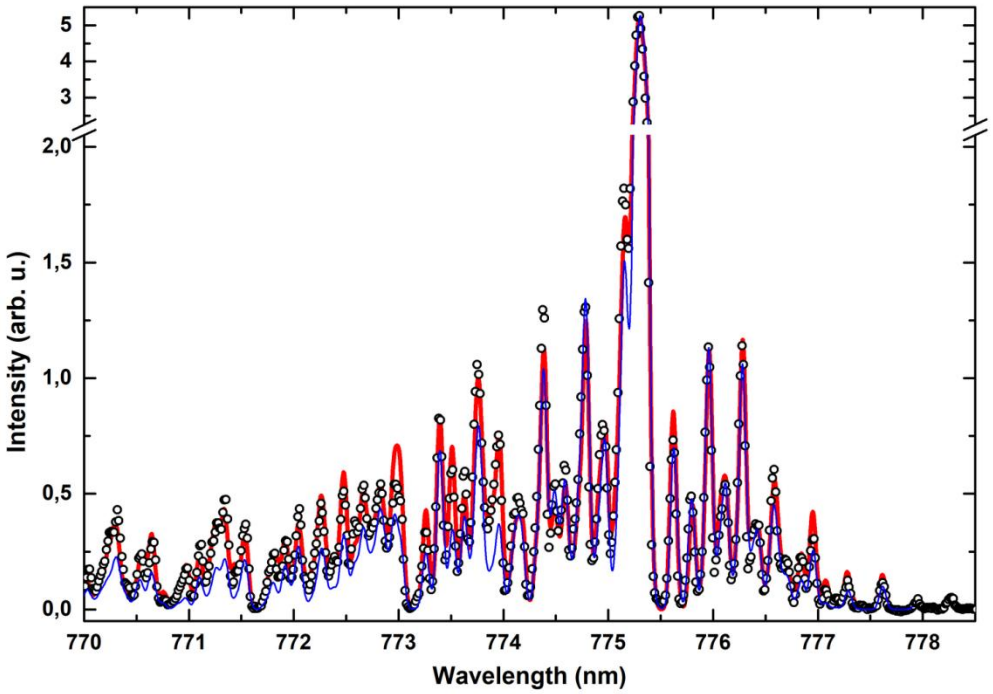

Fig. 7. Comparison of the experimental $N_2(1^+,2\text{-}0)$ spectrum (black circles) from the *top* of the plasma jet (gas mixture $[N_2]/[He]$ = 1/200 as in Fig. 5a), with synthetic spectra with one (blue curve) and two (red curve) temperature distributions.

Spectra of the 2-0 and 3-1 bands of the 1^+system are presented in Figure 8 from the plasma jet (gas mixture $[N_2]/[He]$ = 1/400), recorded at 1 mm above the liquid helium level.

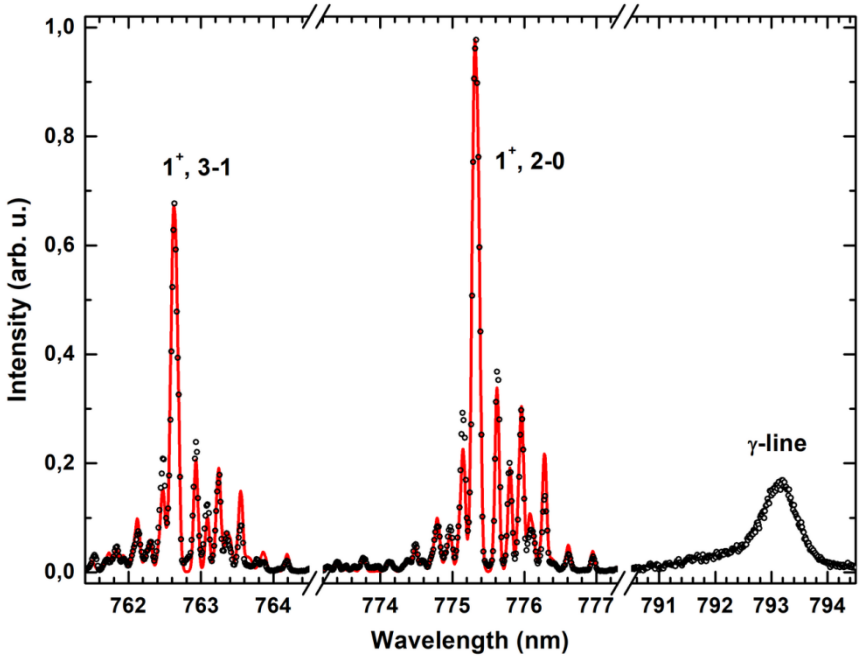

Fig. 8. The experimental spectra (black circles) detected from the *bottom* part of the plasma jet formed by the gas mixture $[N_2]/[He]$ = 1/400 passed through RF discharge area and simulation (red line) of the 2-0 and 3-1 bands of the 1^+ system of N_2 molecules.

The 2-T simulations provide T_r^L=4 K for both vibrational levels and T_r^H=20 and 25 K for vibrational levels v′ =0 and v′ =1, correspondingly. Estimated uncertainties associated with temperatures deduced in 2-T treatment of B-A emission spectrum are 10 % plus 1 K for T_r^L and

20 % plus 5 K for T_r^H. The larger uncertainty for T_r^H is related to the smaller signal to noise ratio in the short wavelengths side of the spectra, from which T_r^H is deduced.

The γ-line shown in Fig. 8 corresponds to the bound-bound transition of the nitrogen anion N^- observable exclusively in solid matrices [88]. The appearance of the γ-line in spectra detected from the bottom part of the plasma jet confirms the presence of solid nanoclusters of molecular nitrogen and, therefore, low temperature (less than 64 K) of the jet.

To summarize:

1) The observed emission of $N_2(1^+;2\text{-}0)$ results from the local production inside the helium gas jet of $N_2(B;2)$ molecules resulting from collisional-radiative cascades of population from higher lying triplet states, which formed probably by N-N recombination and/or dissociative electron-ion recombination (of molecular ions N_3^+ and N_4^+). We believe that the contribution of energy transfer from metastable species $He(^3S_1)$ and $He_2(a^3\Sigma^+_u)$ to the ground state $N_2(X^1\Sigma)$ molecules should be neglected. It is well known that the by-product of their reaction is the Penning ionization, with production of N_2^+ ions [64,65].

2) Following these indirect, multi-channel production ways of $N_2(B;2)$ molecules, it is hard to imagine a possible selectivity regarding the population distribution within the rotational levels of $N_2(B;2)$. Thus, we postulate that the nascent $N_2(B;2)$ is distributed over a large number of rotational levels.

3) With the amount of N_2 added to the feed gas considered in this work (≤0.5 %), collisions with helium atoms and nitrogen only slightly shorten the few μs lifetime of the $N_2(B;2)$ state. Thus, the rotational transferring collisions could be effective enough for modifying the nascent distribution within rotational levels before the emission of $N_2(1^+;2\text{-}0)$ radiation.

4) It is worth noting the high rotational levels may keep partially a memory of their nascent distribution due to the increasing energy gap between adjacent rotational levels with *J* and thus decreasing He-induced transfer coefficients between them (see Eq. 4). It should be emphasized that the energy gap between $J = 5$ and 6 of $N_2(B;2)$ is about 20 cm^{-1}, which correspond to kT~ 30 K. Therefore, a Maxwell–Boltzmann distribution, with $T_r = T_g$ is definitely reached within the low *J* levels during the life time of the $N_2(B;2)$ state while for the high *J* levels T_g may be overestimated. Nevertheless, as one can see from Figures 5c and 8 there were no the high *J* levels observed in the bottom part of jets.

In conclusion, simulations of the recorded rotational distribution of the $N_2(B)$ state with equation (5), T_r^L and T_r^H reveal the local gas temperatures in peripheral (cold) and central (hot) parts of the plasma jet. Moreover, this property is not limited to the vibrational state with v=2 of the $N_2(B)$ state: similar values of T_r^L and T_r^H were obtained also for the 3-1 band of the 1^+system (Fig. 8).

4. Discussion

The temperature of a gas mixture passed through a RF discharge region depends on the pressure, discharge conditions, gas mixture composition and flux. The gas temperature can't be lower than 77 K, the temperature of liquid nitrogen used to precool the gas mixture and remove the local excess heat from the RF discharge area. The plasma jet temperatures at three positions along the plasma jet evaluated from rotational structures of the bands of N_2 molecule and the intensities of the oxygen atom triplet lines are listed in Table 1. Position "Top" is near the exit of the capillary and at about 25 mm about the HeII surface; position "Bottom" being at 1 mm above this surface and "Middle" at 13 mm from it. Obviously, the intensity ratios of oxygen triplet lines provide the highest values at low nitrogen amount (< 0.1 %) in the jet. However, the temperature

deduced from the relative intensities of oxygen 777 nm triplet lines should be considered with caution. We point out that this method provides the gas temperature under the assumption of a total Boltzmann equilibrium within the sub-levels of the $O(^5P_J)$ state. According to the analysis developed in section 3.2, the above assumption is valid only if the collisional transfer rate between sub-levels is much larger than their population decay rate, a condition which holds when the kinetic energy of collision partners is much larger than the energy gaps between $O(^5P_J)$ sub-levels; or if $O(^5P_J)$-He interaction is of van der Waals type, with purely attractive potential curves. The presence of a hump on interaction potentials, even of only a few cm^{-1} height, can act as a barrier on the entrance channel of the sub-levels transfer reaction and invalidate the assumption we made in section 3.2 on non T_g dependence of $\sigma_{J,J'}$ cross-sections. With the diminution of transfer rates, the population mixing times of the sub-levels induced by collision with He will become larger than the lifetime of the $O(^5P_J)$ state and consequently the population distribution between $O(^5P_J)$ sub-levels will depend on their production rates. As pointed out in 3.2, the production rates of sub-levels should be very close to their statistical weights, $2J+1$ and $O(^5P_3)$ atoms, which have the highest energy (see Fig. 3) will be produced with a larger rate than $O(^5P_1)$ atoms populating the lowest energy level. With the helium induced collisional transfers between sub-levels not being efficient enough for the establishment of a Boltzmann equilibrium between them, the population distribution will keep in memory the initial production rates of the sublevels. We can thus conclude that the assumption made in 3.2 relative to the temperature independence of $\sigma_{J,J'}$ cross-sections for collision induced transfers between sub-levels of $O(^5P_J)$ state is not valid at cryogenic temperatures, indicating the presence of small energy barriers on the potential curves of the transient $O(^5P_J)$-He molecule. As one can see in Table 1 the temperature estimated from the triplet of oxygen atom (for the gas mixture $[N_2]/[He] = 1/10000$) may noticeably deviate from the one obtained with PGopher software from the rotational structures of molecular nitrogen, but remains within the temperature obtained by 2-T simulations. The real gas temperature and pressure/density of the environment govern the thermal relaxation rate of oxygen atoms. One can expect that at low pressure the level populations of the $3p^5P$ state may deviate from the Boltzmann distribution law because of its very short life time ≈ 29 ns [45].

Table 1. The plasma jet temperatures along the jet height evaluated from rotational structure of the bands of N_2 molecule and the intensities of the oxygen atom triplet lines.

gas	probe	top	middle	bottom
pure He	O atom			12.5
$[N_2]/[He]$ = 1/10000	O atom	70	36	23
	$N_2(1^+,2\text{-}0)$ PGopher	42±10.5	30±7.5	18±4.5
	$N_2(1^+,2\text{-}0)$ 2-T*	20-100	18-70	8-70
$[N_2]/[He]$ = 1/400	$N_2(1^+,2\text{-}0)$ 2-T*			4-20
	$N_2(1^+,3\text{-}1)$ 2-T*			4-25
$[N_2]/[He]$ = 1/200	N_2(IRA ,8-3) PGopher		35±7	11±2.2
	$N_2(1^+,2\text{-}0)$ PGopher	50±5	38±3.8	14.5±1.5
	$N_2(1^+,2\text{-}0)$ 2-T*	30-120	14-60	5-20

*- the uncertainty in T_r^L and particularly $T_r^H$is rather large due to very low intensity of the spectra of the 2-0 band detected from a plasma jet with the low nitrogen content, 100 ppm (see Fig. 6).

The results listed in Table 1 show the highest temperature values in the helium plasma jet as high as 100-120 K. We should mention also that the temperature of jets expanding into vacuum decreases with lowering of the nitrogen content in the helium gas [16].

The temperatures evaluated from rotational structures of the 2-0 band of the 1^+ system and the 8-3 band of IRAS of molecular nitrogen detected from the middle and bottom parts of the jet do match very well one with another: 38 and 35 K, 14.5 and 11 K, respectively (Table 1). This fact could be expected because of rather long life times of both the $B^3\Pi_g$ and $B'^3\Sigma_u$ states, 10 μs and 25-50 μs, correspondingly [56,57]. Therefore, we can conclude the 1-T method (simulation with PGopher software) is convenient for the gas temperature mapping with high spatial resolution in inhomogeneous plasmas.

As we can see from Table 1, the jet temperatures above the superfluid helium level in the beaker, 4-8 K, are far above the temperature of the bulk HeII, 1.45 K. Such a temperature gap is related to the fact that the jet creates a crater with the depth of 5-10 mm (Fig. 2a). The crater is easily discernible due to the green glow below the HeII level in the beaker. We suggest the gas flow scattered from the HeII surface in the crater is the coldest part of the plasma jet. Unfortunately, our efforts to detect spectra from this diffuse greenish eddy were not successful until now.

We should also mention that spectra of the 2-0 band of the 1^+ system and the 8-3 band IRA system of molecular nitrogen are located very close one to another and cover together only about 10 nm of spectral range (Figure 5). Therefore, both spectra may be detected simultaneously by a simple spectrometer consisting of a linear CCD detector and a grating efficient within the spectral range from 772 to 782 nm providing the spectral resolution of 0.1 nm or better. Such a simple device will be a good diagnostic tool for the temperature determination of helium cryogenic plasmas at temperatures below 100 K in the future.

5. Conclusions

We have proposed and tested two means for temperature determination of the cryogenic helium plasma jets containing small admixtures of either nitrogen (~ 100-1000 ppm) or oxygen (~ 1-10 ppm).

It was shown that the relative intensities of the oxygen triplet 777 nm lines may deviate from the real temperature of the gas in the cryogenic plasma afterglow due to the presence of small energy barriers on the potential curves of the transient $O(^5P_J)$-He molecule and the very short life time, ≈ 29 ns, of the ^5P_J state. Our analysis indicates that these barriers of a few cm^{-1} on the potential curves of the transient $O(^5P_J)$-He molecule, formed during the collision, should limit the collisional transfer rates between the sublevels of $O(^5P_J)$ atom and thus, to the establishment of the Boltzmann equilibrium between them before the emission.

It was proved that the temperature of gas in non-equilibrium cryogenic helium plasmas can be determined from rotational spectra of the 2-0 band of the 1^+ system and the 8-3 band IRA system of molecular nitrogen. The 2-T method allows evaluation of the temperature span within the observation area of inhomogeneous plasma while the 1-T method (PGopher software) gives the rotational temperature of N_2 molecules averaged over the area and is optimal for the gas temperature determination in locally homogeneous plasmas or mapping the temperature of inhomogeneous plasmas with high spatial resolution.

It was determined from rotational structure of the 2-0 band of the 1^+ system of molecular nitrogen that the temperature of the jet entering cold ($T \approx 1.45$ K) dense helium gas changes from 100-120 K at its top of the jet to 4-5 K at its bottom.

The temperature of cryogenic helium plasmas can be monitored by a simple spectrometer (with the resolution better than 0.1 nm) with the working range from 772 to 782 nm due to the compact location of the depleted rotational spectra of the 2-0 and 8-3 bands of the 1^+ and IRA systems of molecular nitrogen, correspondingly.

Acknowledgments

This work was supported by NSF grant DMR 1257565 and by Program for Basic Researches 2013–2020 (project AAAA-A18-118112290069-6).

References

[1] D.W. Tokaryk, R.L. Brooks, and J.L. Hunt, *Phys. Rev. A* **48**, 364 (1993). https://doi.org/10.1103/PhysRevA.48.364

[2] A.B. Callear, R.E. M. Hedges, *Nature* **215**, 1267 (1967). https://doi.org/10.1038/2151267a0

[3] R.L. Brooks, J.L. Hunt, and D.W. Tokaryk, *J. Chem. Phys.* **91**, 7408 (1989). https://doi.org/10.1063/1.457265

[4] S. Yurgenson, C.C. Hu, C. Kim, and J.A. Northby, *Eur. Phys. J. D* **9**, 153-157 (1999). https://doi.org/10.1007/s100530050417

[5] N. Bonifaci, V.M. Atrazhev, V.A. Shakhatov, R.E. Boltnev, K. von Haeften, J. Eloranta, *High Temp.* **55**, 326 (2017). doi: 10.1134/S0018151X1703004X

[6] V.N. Ochkin, S.Yu. Savinov, and N.N. Sobolev, Nonequilibrium distribution of $N_2(C^3\Pi)$ molecules over the rotational levels in a gas discharge. *Sov. Phys. JETP* **48**, 232-237 (1978).

[7] S. Neeser, R. Tietz, M. Schulz, and H. Langhoff, *Z. Phys. D* **31,** 61 (1994). doi: 10.1007/BF01426580

[8] K. Kimura *J. Chem. Phys.* **84**, 2002 (1986). doi: 10.1063/1.450408

[9] Golubovskii Y B, Kulikov V V, Lavrov B P, and Skoblo Y E 1986 *High Temp.* **24** 19-23

[10] Golubovskii Yu B, Siasko A V, and Nekuchaev V O 2020 *Plasma Sources Sci. Technol.* **29**, 065020. https://doi.org/10.1088/1361-6595/ab8fbc

[11] L.G. Mendoza-Luna, N.M.K. Shiltagh, M.J. Watkins, N. Bonifaci, F. Aitken, and K. von Haeften, *J. Phys. Chem. Lett.* **7**, 4666 (2016). doi: 10.1021/acs.jpclett.6b02081

[12] E.B. Gordon, L.P. Mezhov-Deglin, O.F. Pugachev, and V.V. Khmelenko, *Chem. Phys. Lett.* **54**, 282 (1978). doi:10.1016/0009-2614(78)80101-8

[13] Y. Noma, J.H. Choi, T. Tomai, and K. Terashima, *Appl. Phys. Lett.* **93**, 101503(2008). https://doi.org/10.1063/1.2980436

[14] S. Stauss, H. Muneoka, N. Ebato, F. Oshima, D. Z. Pai, and K. Terashima, *Plasma Sources Sci. Technol.* **22**, 025021 (2013). https://doi.org/10.1088/0963-0252/22/2/025021

[15] K. Urabe, H. Muneoka, S. Stauss, O. Sakai, and K. Terashima, *Jap. J. Appl. Phys.* **54**, 106101 (2015). doi: 10.7567/JJAP.54.106101

[16] K.P. Huber and M. Vervloet, *J. Mol. Spectrosc.* **153**, 17 (1992). doi: 10.1016/0022-2852(92)90453-U

[17] V. Singh, A.K. Samanta, N. Roth, D. Gusa, T. Ossenbrüggen, I. Rubinsky, D.A. Horke, and J. Küpper, *Phys. Rev. A* **97**, 032704 (2018). doi: 10.1103/PhysRevA.97.032704

[18] V.V. Khmelenko, S. Mao, A. Meraki, S. Wilde, P. McColgan, R.E.Boltnev,A.A. Pelmenev, D.M. Lee, *Phys. Rev. Lett.* **111**, 183002 (2013). doi: 10.1103/PhysRevLett.111.183002

[19] R.E. Boltnev, I.B. Bykhalo, V.V. Khmelenko, I.N. Krushinskaya, D.M. Lee, P.T. McColgan, S. Sheludiakov, and A.A. Pelmenev, *Low Temp. Phys.* **45**, 732 (2019). doi: 10.1063/1.5111300

[20] A. Trottier, A.I. Jirasek, H.F. Tiedje, and R.L. Brooks, *Phys. Rev. A* **61**, 052504 (2000). doi: 10.1103/PhysRevA.61.052504

[21] A.T. Droegeand P.C. Engelking, *Chem. Phys. Lett.* **96**, 316 (1983). doi: 10.1016/0009-2614(83)80680-0

[22] E. Popov, J. Ahokas, J. Eloranta, and H. Kunttu, *AIP Conference Proceedings* **850**, 384 (2006). doi: 10.1063/1.2354748
[23] D. Ishihara, Y. Noma, S. Stauss, M. Sai, T. Tomai, and K. Terashima, *Plasma Sources Sci. Technol.* **17**, 035008 (2008). doi: 10.1088/0963-0252/17/3/035008
[24] S. Stauss, H. Muneoka, and K. Terashima, *Plasma Sources Sci. Technol.* **27**, 023003 (2018). https://doi.org/10.1088/1361-6595/aaaa87
[25] C. Biloiu, X. Sun, Z. Harvey, and E. Scime, *Rev. Sci. Instrum.* **77**, 10F117 (2006). doi: 10.1063/1.2219392
[26] C. Biloiu, X. Sun, Z. Harvey, and E. Scime, *J. Applied Phys*. **101**, 073303-11 (2007). doi: 10.1063/1.2537448
[27] E.B. Gordon, L.P. Mezhov-Deglin, and O.F. Pugachev, Stabilization of nitrogen atoms in superfluid helium. *JETP Lett.* **19**, 63-65 (1974).
[28] A. Meraki, S. Mao, P.T. McColgan, R.E. Boltnev, D.M. Lee, and V.V. Khmelenko, *J. Low Temp. Phys.* **185**, 269 (2016). doi: 10.1007/s10909-016-1557-1
[29] V.V. Khmelenko, S. Mao, A. Meraki, S.C. Wilde, P.T. McColgan, A.A. Pelmenev, R.E. Boltnev, and D.M. Lee, *J. of Physics: Conference Series* **568**, 032010 (2014). doi: 10.1088/1742-6596/568/3/032010
[30] Wiese, W.L., Smith, M.W., and Glennon, B.M. 1966, NSRDS-NBS 4.
[31] A. Schmidt-Bleker, S. A. Norberg, J. Winter, E. Johnsen, S. Reuter, K. D. Weltmann, and M. J. Kushner, *Plasma Sources Sci. Technol.* **24**, 035022 (2015). doi: 10.1088/0963-0252/24/3/035022
[32] A. Bourdon, T. Darny, F. Pechereau, J-M. Pouvesle, P. Viegas, S. Iseni and E. Robert, *Plasma Sources Sci. Technol.* **25**, 035002 (2016). doi: 10.1088/0963-0252/25/3/035002
[33] I. Jogi, R. Talviste, J. Raud, K. Piip, and P. Paris, *J. Phys. D: Appl. Phys.* **47**, 415202 (2014). doi: org/10.1088/0022-3727/47/41/415202
[34] Q. Xiong, A Yu. Nikiforov, M. A Gonzalez, Ch. Leys and X P. Lu, *Plasma Sources Sci. Technol.* **22**, 015011 (2013). https://doi.org/10.1088/0963-0252/22/1/015011
[35] V. Schulz-von der Gathen, L. Schaper, N. Knake, S. Reuter, K Niemi, T. Gans, and J. Winter, *J. Phys. D: Appl. Phys.* **41**, 194004 (2008). https://doi.org/10.1088/0022-3727/41/19/194004
[36] D. W. Liu, F. Iza and M. G. Kong, *Appl. Phys. Lett.* **95**, 031501 (2009). doi: 10.1063/1.3186073
[37] G. Nayak, N. Sadeghi and P. Bruggeman, *Plasma Sources Sci. Technol*. **28**, 125006 (2019). doi: 10.1088/1361-6595/ab3691
[38] X Y. Liu, X K. Pei, X P. Lu and D W. Liu, *Plasma Sources Sci. Technol.* **23**, 035007 (2014). https://doi.org/10.1088/0963-0252/23/3/035007
[39] R. J.Carman, R.Ganesan and D. M.Kane, *J. Phys. D: Appl. Phys.* **49**, 085201 (2016). https://doi.org/10.1088/0022-3727/49/8/085201
[40] S. Reuter, K. Niemi, V. Schulz-von der Gathen and H F. Dobele, *Plasma Sources Sci. Technol.* **18**, 015006 (2009). https://doi.org/10.1088/0963-0252/18/1/015006
[41] K. Niemi, J. Waskoenig, N. Sadeghi, T. Gans and D. O'Connell, *Plasma Sources Sci. Technol.* **20**, 055005 (2011). https://doi.org/10.1088/0963-0252/20/5/055005
[42] S. Nemschokmichal, R. Tschiersch, and J. Meichsner, *Plasma Sources Sci. Technol.* **25**, 055024 (2016). https://doi.org/10.1088/0963-0252/25/5/055024
[43] J. Waskoenig, K. Niemi, N. Knake, L M. Graham, S Reuter, V. Schulz-von der Gathen and T. Gans, *Plasma Sources Sci. Technol.* **19**, 045018 (2010). https://doi.org/10.1088/0963-0252/19/4/045018
[44] N. Sadeghi, Unpublished
[45] N. Zheng and T. Wang, *Astrophys. J. Suppl. Series* **143**, 231 (2002). doi: 10.1086/342421
[46] A.E. Belikov, O.V. Kusnetsov, and R.G. Sharafutdinov, *J. Chem. Phys.* **102**, 2792 (1995). doi: 10.1063/1.468655

[47] J. Dagdigian, B E. Forch and A W. Miziolek, *Chem. Phys. Lett.* **148**, 299 (1988). https://doi.org/10.1016/0009-2614(88)87276-2
[48] N. Sadeghi, D W. Setser, A. Francis, U. Czarnetzki, and H F. Dobele, *J. Chem. Phys.* **115**, 3144 (2001). https://doi.org/10.1063/1.1388037
[49] V. N. Ochkin, *Spectroscopy of Low Temperature Plasma.* John Wiley & Sons,2009.
[50] P.J. Bruggeman, N. Sadeghi, D.C. Schram, and V. Linss, *Plasma Sources Sci. Technol.* **23**, 023001 (2014). https://doi.org/10.1088/0963-0252/23/2/023001
[51] R. Engeln, B.L.M. Klarenaar, and O. Guaitella, 2020 *Plasma Sources Sci. Technol.* **29**, 063001. https://doi.org/10.1088/1361-6595/ab6880
[52] S.G. Belostotskiy, T. Ouk, V.M. Donnelly, D.J. Economou and N. Sadeghi, *J. Appl. Phys.* **107**, 053305 (2010). https://doi.org/10.1063/1.3318498
[53] Q. Wang, F. Doll, V.M. Donnelly, D.J. Economou, N. Sadeghi and F. Franz, *J. Phys. D: Appl. Phys.* **40**, 4202 (2007).
[54] C. Douat, I. Kacem, N. Sadeghi, G. Bauville, M. Fleury and V. Puech, *J. Phys. D: Appl. Phys.* **49**, 285204 (2016).
[55] T. Dufour, L.J. Overzet, R. Dussart, L.C. Pitchford, N. Sadeghi, P. Lefaucheux, M. Kulsreshath and P. Ranson, *Eur. Phys. J. D* **60**, 565 (2010).
[56] L.G. Piper, K. W. Holtzclaw, B.D. Green, and W.A.M. Blumberg, *J. Chem. Phys.* **90**, 5337 (1989).
[57] A. Lofthus and P.H. Krupenie, *J. Phys. Chem. Ref. Data* **6**, 113 (1977).
[58] F.C. Parra-Rojas, M. Passas, E. Carrasco, A. Luque, I. Tanarro, M. Simek, and F.J. Gordillo-Vazquez, *J. Geophys. Res. Space Phys.* **118**, 4649 (2013). doi: 10.1002/jgra.50433
[59] R.E. Boltnev, I.B. Bykhalo, I.N. Krushinskaya, A.A. Pelmenev, V.V. Khmelenko, S. Mao, A. Meraki, S.C. Wilde, P.T. McColgan, and D.M. Lee, *J. Phys. Chem. A* **119**, 2438 (2015). doi: 10.1021/jp508534t
[60] C.M. Western, *J. Quant. Spectrosc. Radiat. Transf.* **186**, 221 (2016). doi: 10.1016/j.jqsrt.2016.04.010
[61] C.M. Western, L. Carter-Blatchford, P. Crozet, A.J. Ross, J. Morville, and D.W. Tokaryk, *J. Quant. Spectrosc. Radiat. Transf.* **219**, 127(2018). doi: 10.1016/j.jqsrt.2018.07.017
[62] A. Shadee, *Astron. & Astrophys.* **41**, 213-215 (1975).
[63] C. Effantin, C. Amiot, and J. Verges, *J. Mol. Spectrosc.* **76**, 221-265 (1979).
[64] J-M. Pouvesle, T. Darny, T. Maho, V. Puech, C. Douat, S. Dozias and E. Robert, *Plasma Medecine* **8**, (2018) 83.
[65] J-M. Pouvesle, A. Bouchoule, and J. Stevefelt, *J. Chem. Phys.* **77** (1982) 817.
[66] J A. Guthrie, R C. Chaney and A J. Cunningham, *J. Chem. Phys.* **95** (1991) 930.
[67] K D. Bayes and G B. Kistiakowsky, *J. Chem. Phys.* **32** (1960) 992.
[68] N. Sadeghi, C. Foissac and Ph. Supiot, *J. Phys. D: Appl. Phys.* **34**, 1779 (2001).
[69] H. Partridge, S R. Langhoff and C W. Bauschlicher, Jr, *J. Chem. Phys.* **88** (1988) 3174.
[70] Ch. Ottinger and A F. Vilesov, *J. Chem. Phys.* **103** (1995) 9929.
[71] R. Bachmann, Ch. Ottinger, and A F. Vilesov, *J. Chem. Phys.* **99** (1993) 3262.
[72] R. Bachmann, X. Li, Ch. Ottinger, A F. Vilesov, and V. Wulfmeyer, *J. Chem. Phys.* **98** (1993) 8606.
[73] N. Sadeghi and D W. Setser, *J. Chem. Phys.* **79** (1983) 2710.
[74] A. Rotem, I. Nadler, and S. Rosenwaks, *J. Chem. Phys.* **76** (1982) 2109.
[75] L. G. Piper*J. Chem. Phys.* **91**, 864 (1989). doi: 10.1063/1.457138
[76] L. G. Piper*J. Chem. Phys.* **88**, 6911 (1988). doi: 10.1063/1.454388
[77] G. Herzberg, *Molecular spectra and molecular structure*, Vol. 1, Van Nostrand Reinhold, New York, (1950)
[78] D W Setser, D H. Stedman and J A. Coxon, *J. Chem. Phys.* **53** (1970) 1004.
[79] L. G. Piper *J. Chem. Phys.* **97**, 270 (1992). doi: 10.1063/1.463625
[80] A. Rotem, I. Nadler, and S. Rosenwaks, *Chem. Phys. Lett.* **83** (1981) 281.

[81] J A. Barnes, M. Keil, R E. Kutina, and J C. Polanyi, *J. Chem. Phys.* **72** 6306 (1980). doi: 10.1063/1.439047
[82] J. Derouard and N. Sadeghi, *J. Chem. Phys.* **81** (1984) 3002.
[83] T A. Bruner, R D. Driver, N. Smith, and D E. Pritchard, *J. Chem. Phys.* **70** (1979) 4155.
[84] J. Derouard and N. Sadeghi, *Chem. Phys.* **88** (1984) 171.
[85] A E. De Pristo, S D. Augustin, R. Ramaswamy and H. Rabitz, *J. Chem. Phys.* **71** (1979) 850.
[86] B J. Whitaker and P. Brechignac, *Chem. Phys. Lett.* **95** (1983) 407.
[87] J. Derouard and N. Sadeghi, *Chem. Phys. Lett.* **102** (1983) 324.
[88] R.E. Boltnev, I.B. Bykhalo,I.N. Krushinskaya, A.A. Pelmenev,S. Mao, A. Meraki, P.T. McColgan, D.M. Lee, and V.V. Khmelenko, *Phys. Chem. Chem. Phys.***18**, 16013 (2016). doi: 10.1039/c6cp01080f